Research on a Novel Clutter Map Constant False Alarm Rate Detector Based on Power Transform

Bangzhen XU, Yiqin CHEN, Hong GU, Weimin SU

Dept. of Electronic Engineering, School of Electronic and Optical Engineering,
Nanjing University of Science and Technology, Xiao Ling Wei Street 200, 21000 Nanjing, People's Republic of China

gh_student_sub@126.com

Submitted March 24, 2021 / Accepted November 17, 2021

Abstract. *A power transform-based clutter map constant false alarm rate (CM/PT-CFAR) algorithm is proposed to improve the detection performance to the weak target in multiple persisting targets situations. In the CM/PT-CFAR detector, the radar dataset obtained at each scan is normalized and multiplied by a scale factor, and then fed to the power transform operation. The transformed dataset is divided into two parts with a numerical value of 1 as the boundary. The part exceeding 1 is fed to update the scale factor, while the other is used for updating the detection threshold. Because transcendental integrals are produced in the derivation process, an accurate analytical expression of detection probability for CM/PT-CFAR is non-existent. Hence a third-order Taylor expansion operation is introduced to approximate the result. The detection performance of CM/PT-CFAR under various conditions is evaluated and compared with those of other CM/-CFAR detectors. The advantage of CM/PT-CFAR is the detection for weak targets, especially in complex detection situations. The proposed algorithm remains a relatively stable computation load in different cases, which is beneficial for practical application.*

Keywords

Constant false alarm rate, clutter map, power transform, weak target detection, multiple persisting targets, detection probability

1. Introduction

Constant false alarm rate (CFAR) detection is an important part of automatic detection in modern radar systems. The basic framework of CFAR is to maintain the preset false alarm probability by estimating the background power of the radar scene and multiplying it by a constant scale factor to obtain a detection threshold that can adapt to various clutter environments [1], [2]. CFAR detectors can be divided into two categories according to different background power estimation methods: spatial processing-based CFAR detectors and temporal processing-based CFAR detectors [3], [4].

For spatial processing-based CFAR detectors, the outputs of nearby cells (range/Doppler) are averaged to obtain a background estimation which is used for thresholding [5], [14]. Common spatial processing-based CFAR detectors, such as mean-level CFAR (ML-CFAR) detectors and rank-ordering CFAR detectors can achieve excellent detection performance in a homogeneous environment, but also suffer from performance degradations caused by non-homogeneous environments such as multiple targets situations or clutter edge environments [6], [7]. These detectors often achieve a poor false alarm control capacity at clutter edges [8], [9].

Temporal processing-based CFAR detectors are based on different concepts, where the background estimation is obtained by processing the output of multiple scans within each resolution cell. The estimation is updated scan-by-scan and used to compute the detection threshold for the map cell at the next scan [2], [10]. This temporal processing-based CFAR technique is also known as clutter map CFAR (CM-CFAR) for utilizing resolution cells of the clutter map. Compared with the spatial processing-based CFAR algorithms, CM-CFAR has the advantages of robustness in the presence of multiple targets and immunity to clutter edge environments [11–13].

The classic CM-CFAR was first analyzed by Nitzberg et al. It utilizes digital exponential weighting of prior scan measurements to obtain the background estimation in each resolution cell [14]. The derived algorithms of CM-CFAR usually deal with the investigated resolution cells by average or orderly processing. The cell average CM-CFAR (CACM-CFAR) detector updates the detection threshold by filtering the average of returns within map cells at each scan. CACM-CFAR has the advantage of good detection performance in a homogeneous environment, but in the case of persisting targets in the clutter map it suffers from a performance degradation caused by target-masking effect, where the detection threshold raises with the increased number of scans [15]. For the order of statistic CM-CFAR (OSCM-CFAR) detector based on a different concept, the kth ranked resolution cell is chosen for detection threshold updating. OSCM-CFAR performs more robustly in the case of persisting targets compared with CACM-CFAR at the cost of a small CFAR loss in a homogeneous environment

DOI: 10.13164/re.2022.0114

[16]. In [17], the authors proposed a hybrid clutter map/L-CFAR (CM/L-CFAR) detector, where the returns from each resolution cell were preliminarily processed through an L-filter before being fed to the background estimation. This algorithm preserves immunity to spatial discontinuity points such as a clutter map edge environment while enhancing robustness in the persisting target case, but suffers from a limited CFAR loss in a homogeneous environment. A scan-by-scan averaging CFAR (SSA-CFAR) detector which selects the maximal resolution cell for updating the detection threshold is analyzed in [11]. SSA-CFAR achieves robust performance with respect to spatial environment conditions, but suffers from a performance degradation caused by self-masking targets. In [18], a switching IIR CFAR (SIIR-CFAR) detector that switches between two exponential smoothers with different time constants to leverage the conflicting requirements of homogeneous and nonhomogeneous environments is proposed. It has the advantages of maintaining good detection performance in homogeneous environments and fast adaption to spatial discontinuity points such as clutter edge environments. To achieve a reasonable trade-off between the homogeneous detection loss and nonhomogeneous detection improvement, the authors proposed a CM-CFAR detector based on the maximal resolution cell, which is named CM/MRC-CFAR in [19]. The core of this algorithm is to multiply the maximal resolution cell within each scan by a scale factor to construct a comparison threshold and count the number of remaining cells that do not exceed this threshold. According to the preset tolerance of the target number, the appropriate resolution cells are selected to update the detection threshold. This algorithm has the advantages of a low CFAR loss in homogeneous environment and robust detection performance in persisting targets situations.

In [20–24], the authors studied the CFAR performance in Weibull and lognormal backgrounds. In addition, new techniques such as machine learning are applied to CFAR detectors in [25–27].

To detect the weak targets which enter the radar scene successively and persist for several scans, a CM-CFAR detector based on power transform (i.e. CM/PT-CFAR) is proposed in this paper. In the proposed algorithm, the radar dataset is firstly processed by a specific scale transformation and then divided into two parts, with one part used for updating the scale factor, and the other fed to the background estimation. Then, the power transform is imposed to increase the separability between the target echoes and clutters. The power transform can prevent the amplification of clutter intensity, and keep it under the detection threshold. As such, the false alarms caused by clutters decrease and the weak target detection performance can be enhanced. The proposed CM/PT-CFAR method can achieve a robust detection performance for weak targets, especially when multiple persisting targets enter the radar scene successively.

The remainder of this paper is organized as follows. The algorithm flowchart of CM/PT-CFAR is presented in Sec. 2. The detection probability (*Pd*) of CM/PT-CFAR is derived from a third-order Taylor expansion operation, as described in Sec 3. The performance evaluation and parameter investigation of CM/PT-CFAR in various environments is presented in Sec. 4.

2. Description of CM/PT-CFAR Process

The block diagram of the CM/PT-CFAR algorithm is shown in Fig. 1. Square-law detected signals are organized corresponding to the adjacent M resolution cells. For the nth scan, the return signals from M cells are denoted as:

$$\boldsymbol{x_M} = \left[x_1(n), x_2(n), \ldots, x_M(n) \right]. \tag{1}$$

It is assumed that the statistics of the return envelope are Gaussian for the sum of thermal noise plus clutter plus target, and the signal from each resolution cell is statistically independent on a scan-by-scan basis. The target return corresponds to a Swerling II target fluctuation model. Thus, the probability density function (pdf) of each resolution cell is:

$$f(x) = \frac{1}{\lambda(1+\sigma)} \mathrm{e}^{-x/\lambda(1+\sigma)}, \; x \geq 0 \tag{2}$$

where λ is the sum of the thermal noise and clutter power, and σ is the average signal-to-noise ratio (SNR).

For CM/PT-CFAR, at the nth scan, the data of return signal vector $\boldsymbol{x_M}$ are reordered. Each element in $\boldsymbol{x_M}$ is arranged in a small to large order, and a new order vector $\boldsymbol{x_{(M)}}$ is obtained and denoted as:

$$\boldsymbol{x_{(M)}} = \left[x_{(1)}(n), x_{(2)}(n), \ldots, x_{(M)}(n) \right]. \tag{3}$$

It has $x_{(1)}(n) \leq x_{(2)}(n) \leq \ldots \leq x_{(M)}(n)$, after which element $x_{(M)}(n)$ is multiplied by a scale factor γ with $x_{(1)}(n)/x_{(M)}(n) < \gamma \leq 1$. An intermediate vector $\boldsymbol{y_m} = [y_1(n), y_2(n), \ldots, y_M(n)]$ is obtained using the following equation:

$$y_k(n) = \frac{x_{(k)}(n)}{\gamma \cdot x_{(M)}(n)}, \; k = 1, 2, \cdots, M \cdot \tag{4}$$

Obviously, it has $y_1(n) \leq y_2(n) \leq \ldots \leq y_k(n) < 1 \leq y_{k+1}(n) \leq \ldots \leq y_M(n)$, which is an important basis for the following process. A vector $\boldsymbol{z_m} = [z_1(n), z_2(n), \ldots, z_M(n)]$ is then obtained by a power transform as follows:

$$z_k(n) = \left[y_k(n) \right]^v, \;\; k = 1, 2, \cdots, M \tag{5}$$

where v is a power exponent between 0 and 1. The M elements of $\boldsymbol{z_m}$ are partitioned into two sets S_0 and S_1, according to the following comparison:

$$z_k(n) \underset{S_0}{\overset{S_1}{\gtrless}} 1, \;\; k = 1, 2, \cdots, M \; . \tag{6}$$

The dataset S_0 is utilized to update the detection threshold, while the dataset of S_1 is channeled back into

updating the scale factor γ, which is the ratio of root-mean-square to maximum of S_1.

The number of elements partitioned into S_0 is denoted as m_0, and a statistic $q(n)$ is computed as follows:

$$q(n)=\frac{1}{m_0}\sum_{z_k(n)\in S_0} z_k(n)\cdot \tag{7}$$

The sequence $q(n)$ is subsequently fed to a single-pole autoregressive (AR) filter with impulse response $h(n)$, leading to the estimation of background noise and clutter power to the resolution cell at the nth scan. The filter output is the background estimate which is denoted as $\hat{p}(n)$, it has

$$\hat{p}(n)=q(n)*h(n) \tag{8}$$

where * denotes convolution and the impulse response $h(n)$ is expressed as follows:

$$h(n)=\alpha(1-\alpha)^n,\ n>0,\ 0<\alpha<1. \tag{9}$$

For the (n+1)th scan, a target present decision in the kth resolution cell is made if

$$z_k(n+1)>T\cdot\hat{p}(n),\ k=1,2,\cdots,M \tag{10}$$

where T is a constant chosen to set the false alarm rate at the desired level.

It is obvious from the entire process that the most notable difference between CM/PT-CFAR and traditional CFAR algorithms is that the former has additional data process steps, corresponding to (4) and (5). The power transform described in (5) is commonly used to reduce the masking effect of strong scattering points on weak scattering points in radar target recognition. Analogously, CM/PT-CFAR uses a power transform to increase the separability between the resolution cells that contain targets (target cells for short) and those exclusive of targets (clutter cells for short). This operation reduces the target self-masking effect, and improves the detection performance in situations where moving targets enter and persist in the clutter map cells.

The theoretical basis of power transform is that random variables subject to an arbitrary probability distribution can approach a Gaussian distribution by proper power transformations. Therefore, in the process of target detection, power transform changes the pdf of the original dataset, which has an uncertain impact on the detection accuracy. In order to ensure the stable detection performance, elements in vector $\boldsymbol{x}_{(m)}$ is normalized and multiplied by a scale factor to obtain $\boldsymbol{y}_m$, as described in (4). Elements in $\boldsymbol{y}_m$ are divided into two parts with a numerical value of 1 as the boundary. According to the mathematical characteristics of power transform, elements in vector $\boldsymbol{z}_m$ and $\boldsymbol{y}_m$ are divided on the same basis, thereby averting the negative impact caused by power transform on the subsequent steps. For vector $\boldsymbol{z}_m$, elements exceeding 1 are fed back to update the scale factor γ while the others are used to update the detection threshold.

When a target enters the clutter map and persists over a number of scans, the detection threshold increases accordingly, causing deterioration of the detection performance. Analogously, the persisting strong targets lead to an increased detection threshold, which would degrade the subsequent detection performance of weak targets. Assume that the clutter map contains several strong targets up to the nth scan, and a new weak target appears at the next scan. CM/PT-CFAR reduces the discrepancies between echo intensities of different targets by power transform. This algorithm, meanwhile, ensures that the whole clutter map is processed in equal proportion before being fed to power transform, which avoids the false alarm caused by amplifying the clutter units. Consequently, CM/PT-CFAR has better detection performance for weak targets without increasing false alarm probability.

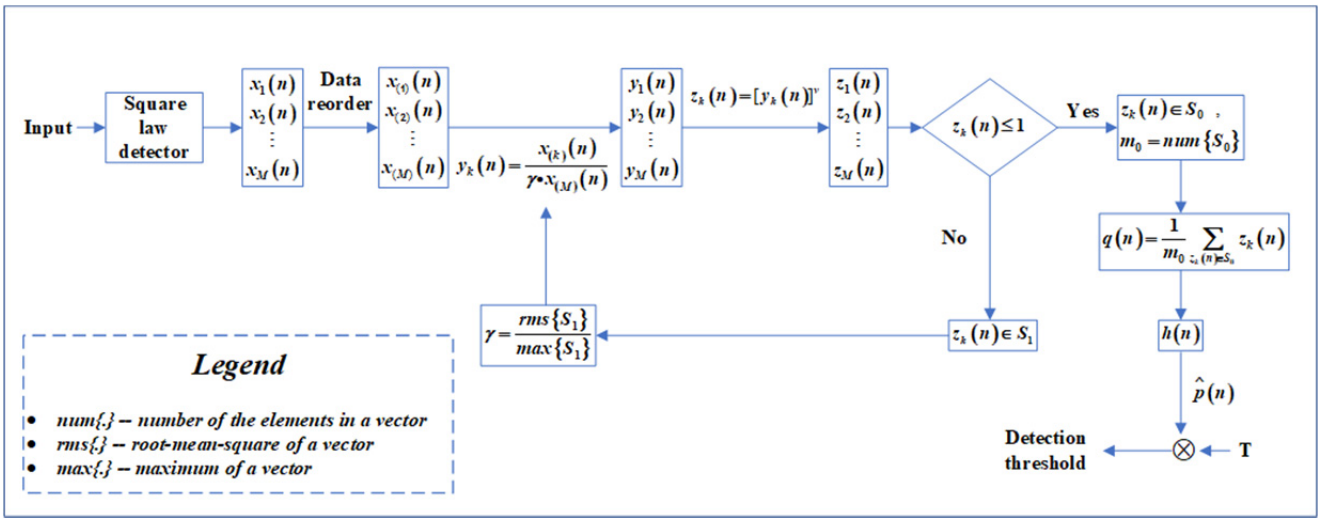

Fig. 1. Block diagram of CM/PT-CFAR algorithm.

3. Mathematical Model of CM/PT-CFAR Algorithm

It is assumed that the returns of each resolution cell are independent from cell to cell, and the clutter map remains in a homogeneous clutter environment up to the nth scan. From the (n+1)th scan, N ($1 \le N < M$) moving targets with the same SNR σ enter the clutter map successively and persist in the respective resolution cell for L scans. For CM/PT-CFAR, the probability of target existence in the kth resolution cell at the (n+L+1)th scan is

$$\begin{aligned} P_{\mathrm{d}} &= E_{z_k(n+L+1)}\left\{\mathrm{Prob}\left[z_k\left(n+L+1\right) > T\cdot\hat{p}\left(n+L\right)\right]\right\} \\ &= \int_0^{+\infty}\frac{1}{\lambda\left(1+\sigma\right)}\mathrm{e}^{-z/\lambda(1+\sigma)}\int_0^{z/T} f_{\hat{p}(n+L)}\left(\hat{p}\right)\mathrm{d}\hat{p}\mathrm{d}z \\ &= \Phi_{\hat{p}(n+L)}\left[\frac{T}{\lambda\left(1+\sigma\right)}\right] \end{aligned} \tag{11}$$

where $E_z\{\cdot\}$ denotes the mathematical expectation of variable z, $f_{\hat{p}(n+L)}(\hat{p})$ is the pdf of variable $\hat{p}(n+L)$, and $\Phi_{\hat{p}(n+L)}(t)$ is the moment generating function (MGF) of $\hat{p}(n+L)$.

From (11), we can draw the conclusion that the probability of target existence is determined by the MGF of the background estimate. Combining the convolution operation of (8) with the properties of the MGF, we obtain

$$\Phi_{\hat{p}(n+L)}\left(t\right) = \prod_{k=0}^{+\infty}\Phi_{q(n+L-k)}\left[h\left(k\right)\cdot t\right] \tag{12}$$

where $\Phi_{q(n+L-k)}(t)$ is the MGF of variable $q(n+L-k)$.

In order to further expand this formula, two MGFs $\Phi_{qH}(t)$ and $\Phi_{qI}(t)$ are introduced. $\Phi_{qH}(t)$ denotes the MGF of $q(l)$ when the resolution cell is in a homogeneous environment at the lth scan, while $\Phi_{qI}(t)$ denotes the MGF of $q(l)$ when targets enter the resolution cell at the lth scan. Because the clutter map remains homogeneous up to the nth scan and then turns into a target-entering scenario from the (n+1)th to (n+L)th scan, Equation (12) can be rewritten as follows:

$$\Phi_{\hat{p}(n+L)}\left(t\right) = \prod_{k=0}^{L-1}\Phi_{qI}\left[h\left(k\right)\cdot t\right]\cdot\prod_{k=L}^{+\infty}\Phi_{qH}\left[h\left(k\right)\cdot t\right]. \tag{13}$$

Before deriving the expressions of $\Phi_{qH}(t)$ and $\Phi_{qI}(t)$, several preprocess measures are taken. To simplify the expression, vector $\boldsymbol{z_m}$ obtained at the lth scan is rewritten as $\mathrm{z} = [z_1, z_2, \ldots, z_m]$, where N elements from target cells are denoted as $zt_1, zt_2, \ldots, zt_N$ and M–N elements from clutter cells are denoted as $zc_1, zc_2, \ldots, zc_{M-N}$. For simplification, we set $zt_1 \le zt_2 \le \ldots \le zt_N$ and $zc_1 \le zc_2 \le \ldots \le zc_{M-N}$. The joint pdf of N target returns and M–N clutter echoes can be derived as follows:

$$\begin{aligned} &f_{ZT_1,ZT_2,\ldots,ZT_N,ZC_1,ZC_2,\ldots,ZC_{M-N}}\left(zt_1, zt_2, \ldots, zt_N, zc_1, zc_2, \ldots, zc_{M-N}\right) \\ &\quad = N!\left(M-N\right)!\prod_{i=1}^{N} f_T\left(zt_i\right)\cdot\prod_{j=1}^{M-N} f_C\left(zc_j\right) \end{aligned} \tag{14}$$

where

$$f_{\mathrm{T}}\left(z\right) = \frac{z^{(1-v)/v}}{\lambda v\left(1+\sigma\right)}\mathrm{e}^{-z^{(1/v)}/\lambda(1+\sigma)} \tag{15}$$

and

$$f_{\mathrm{C}}\left(z\right) = \frac{z^{(1-v)/v}}{\lambda v}\mathrm{e}^{-z^{(1/v)}/\lambda}. \tag{16}$$

The two functions above are power-transformed pdfs corresponding to the target cells and clutter cells, respectively. The derivation process is presented in Appendix A.

According to the previous preprocess measures, the situations that $zt_N \ge zc_{M-N}$ and $zt_N < zc_{M-N}$ are mutually exclusive events, thus $\Phi_{qI}(t)$ can be rewritten as:

$$\begin{aligned} \Phi_{qI}\left(t\right) = &\\ &= \sum_{m_0=0}^{M-1}\sum_{l=N_0}^{N_1}\Phi_I\left(t\,|\,m_0, l, zt_N \ge zc_{M-N}\right) \\ &\quad + \sum_{m_0=0}^{M-1}\sum_{l=N_2}^{N_3}\Phi_I\left(t\,|\,m_0, l, zt_N < zc_{M-N}\right) \end{aligned} \tag{17}$$

where

$$N_0 = \max\left(0, m_0 - M + N\right), \tag{18}$$

$$N_1 = \min\left(m_0, N-1\right), \tag{19}$$

$$N_2 = \max\left(0, m_0 - M + N + 1\right), \tag{20}$$

$$N_3 = \min\left(m_0, N\right). \tag{21}$$

The sub-item $\Phi_I(t|m_0, l, zt_N \ge zc_{M-N})$ represents the MGF of $q(l)$ under the condition that l target returns are partitioned into dataset S_0 and the maximum value of target returns exceeds the maximum value of clutter echoes. N_0 and N_1 are the possibly smallest and largest numbers of target returns in this situation, respectively. In contrast, $\Phi_I(t|m_0, l, zt_N < zc_{M-N})$ represents the MGF of $q(l)$ when l target returns are partitioned into dataset S_0 and the maximum value of clutter echoes exceeds the maximum value of the target returns. N_2 and N_3 are the possibly smallest and largest numbers of target returns in this situation, respectively.

The MGF $\Phi_{qH}(t)$ can be rewritten in a similar structure. Note that since $\Phi_{qH}(t)$ corresponds to a homogeneous environment, we can set targets number N and SNR σ in the expression of $\Phi_{qI}(t)$ to 0, so as to simplify the derivation of $\Phi_{qH}(t)$.

The detailed derivation of P_{d} is too cumbersome to be presented in this section. Thus, we show a flowchart of derivation process in Fig. 2. See Appendix B for the specific process. Note that transcendental integrals are produced in the derivation, thus a third-order Taylor expansion operation is used to approximate the accurate analytical expression.

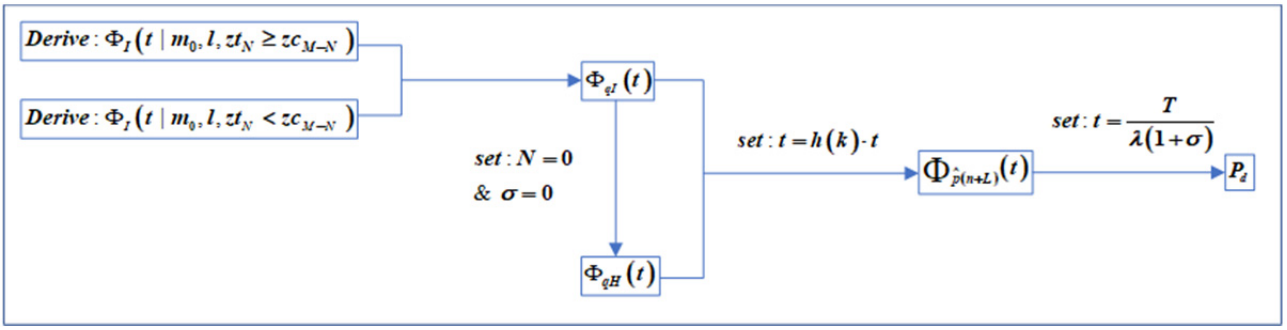

Fig. 2. Flowchart of the derivation process.

4. Experimental Results and Analysis

To evaluate the detection performance of the proposed algorithm, the effects of CM/PT-CFAR are compared with those of other CFAR algorithms. In addition, the key factor which influences the property of CM/PT-CFAR is studied. Before we carry out the experiments, the parameter set of CM/PT-CFAR is designed through a case study.

4.1 Parameter Design through a Case Study

According to the expression of detection probability P_d (see Appendix B), when the size of map cell M and the weight coefficient α of $h(n)$ are given, the detection performance of CM/PT-CFAR depends on two parameters v and T. Assume that $M = 8$ and the desired false-alarm probability $P_F = 1 \times 10^{-5}$. For the single-pole AR filter, since a smaller α corresponds to a longer data window to estimate the clutter power [14], [21], a weight coefficient is taken in the following experiment. The parameter design method proposed in [19] is used, which achieves a reasonable trade-off between the homogeneous detection loss and performance improvement in nonhomogeneous case. The design procedure includes the following steps:

Step 1: For each value of $v \in [0.03, 1]$, based on (B8) (see Appendix B) on condition that L, N, and σ are set to 0, the corresponding threshold factor T is obtained and shown in Tab. 1.

Step 2: For each set of (v,T) in Tab. 1, compute the corresponding P_d of a target in a homogeneous environment by (B8), with $L = 0$, $N = 0$, and $\sigma = 100$. The detection curve is shown in Fig. 3.

Step 3: For each set of (v,T) in Tab. 1, compute the corresponding P_d of a target in multiple persisting targets situations by (B8), with $L = 30$, $N = 2$, and $\sigma = 100$. The detection curve is shown in Fig. 3.

Step 4: Figure 3 also presents the simulation results by the Monte Carlo method, corresponding to the curves in step 2 and step 3. The curves computed by (B8) coincide well with the simulation results. This indicates that it is feasible to use a third-order Taylor expression to approximate the accurate analytical expression. On the curve of $L = 30$ and $N = 2$, when v increases from 0.03 to 0.2385, the corresponding P_d increases sharply from 0 to 84.47%.

v	0.03	0.0442	0.0625	0.0884	0.125
T	4.786	4.786	4.788	4.793	4.793
v	0.1768	0.1895	0.2031	0.2176	0.2385
T	4.871	4.871	4.875	4.875	4.991
v	0.25	0.2679	0.2872	0.3078	0.3299
T	4.991	5.015	5.102	5.481	5.842
v	0.3536	0.5	0.7071	1	
T	6.239	8.157	12.301	16.965	

Tab. 1. Threshold factor T versus power exponent v, for $P_F = 10^{-5}$, $M = 8$ and $\alpha = 0.125$.

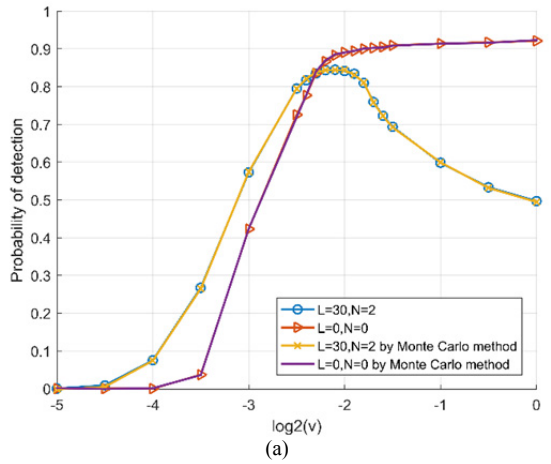

(a)

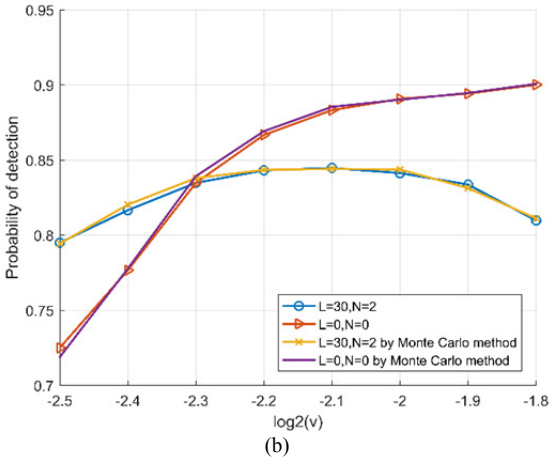

(b)

Fig. 3. Detection performance of CM/PT-CFAR for different values of v: (a) logarithmic form of v is taken as the X-axis; (b) partial curves for observation.

As v continues to increase from 0.25 to 1, the P_d rapidly decreases from 84.13% to 49.66%. Meanwhile, on the curve of $L = 0$ and $N = 0$, the P_d first shows a period of rapid growth, and then maintains a slow rate of increase. As v exceeds 0.2385, the P_d slightly increases from 88.54% to 92.11%. Considering the two situations above, we finally select $v = 0.2385$ because it provides a suitable trade-off between the homogeneous detection loss and performance improvement in nonhomogeneous case.

In summary, the parameter set for CM/PT-CFAR at $P_F = 1 \times 10^{-5}$ is ($M = 8$, $\alpha = 0.125$, $v = 0.2385$, $T = 4.991$). A specific analysis of how the power exponent v influences the detection probability is discussed in Sec. 4.4.

4.2 Detection Performance Evaluation

In this section, the detection performances of CM/PT-CFAR in two types of situations is evaluated and compared with those of CACM-CFAR, OSCM-CFAR, CM/L-CFAR and CM/MRC-CFAR. The parameters of CM/PT-CFAR are set in the previous section. For CM/MRC-CFAR, the parameters are set according to [19]. To ensure that both OSCM-CFAR and CM/L-CFAR can tolerate up to two targets at each scan, the sixth-ranked resolution cell at each scan is used to update the detection threshold for OSCM-CFAR and the censoring depth of CM/L-CFAR at each scan is set to two. The detection probabilities of all the CM-CFAR detectors are obtained by the Monte Carlo method.

4.2.1 Homogeneous Clutter Environment

The detection probability curves of all the CFAR algorithms above are presented in Fig. 4. It is observed that in a homogeneous clutter environment, CACM-CFAR achieves the highest detection probability in the entire SNR range. CM/PT-CFAR performs better than OSCM-CFAR and CM/L-CFAR. Because CM/PT-CFAR does not use all the resolution cells to update the detection threshold, the performance of CM/PT-CFAR is slightly lower than those of CACM-CFAR and CM/MRC-CFAR.

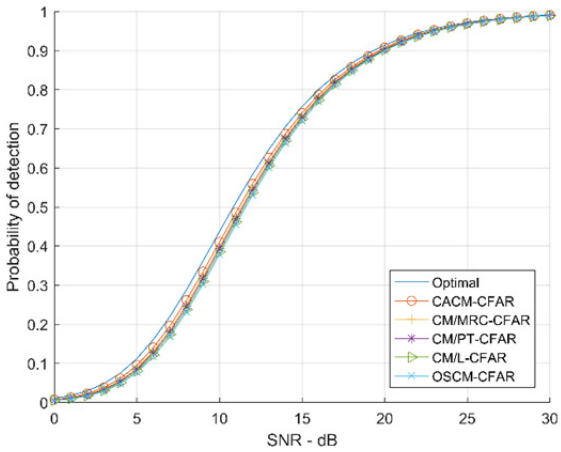

(a)

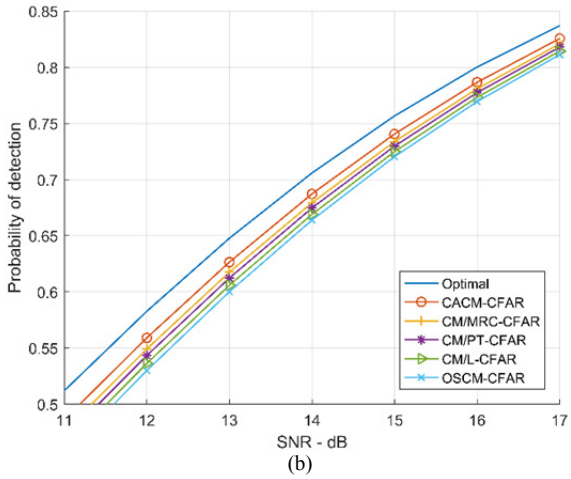

(b)

Fig. 4. Detection performance of various CFAR algorithms in a homogeneous clutter environment: (a) global view; (b) partial curves for observation.

4.2.2 Multiple Persisting Targets Situation

The performances of various CFAR algorithms in the situation that one target enters the clutter map and persists in a certain resolution cell for $L = 10$ scans are shown in

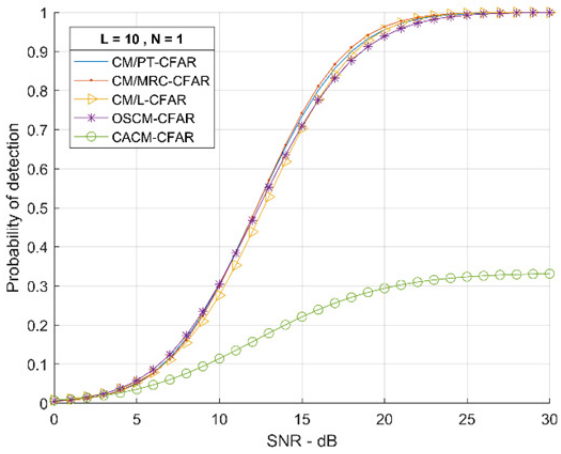

(a)

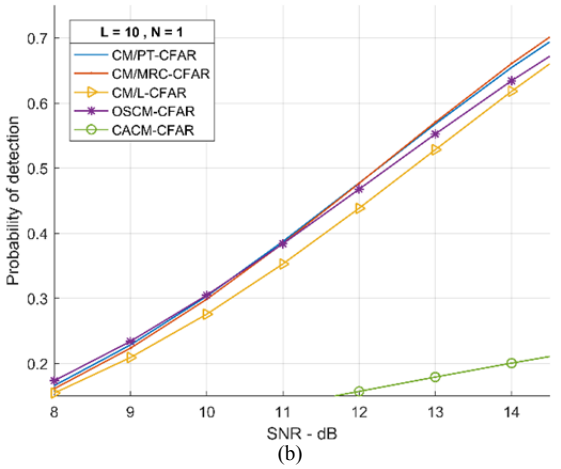

(b)

Fig. 5. Detection performance of various CFAR algorithms in the situation of one target persisting for ten scans: (a) global view; (b) partial curves for observation.

Fig. 5. When the SNR increases from 0 to 10 dB, the detection probability of CM/PT-CFAR is higher than that of CM/L-CFAR, and slightly lower than that of OSCM-CFAR. In the SNR range beyond 11 dB, the detection performance of CM/PT-CFAR tends to exceed that of OSCM-CFAR and remains similar to that of CM/MRC-CFAR. Note that CACM-CFAR achieves poor performance in persisting targets situation and only gives a maximum 33.65% detection probability at SNR = 30 dB.

In the situation of two targets persisting in the same resolution cell for $L = 30$ scans, the detection probability curves of CM/PT-CFAR, CM/MRC-CFAR, CM/L-CFAR and OSCM-CFAR are given in Fig. 6. Since CACM-CFAR is unable to detect targets effectively in this situation, its detection performance is not evaluated here. Obviously, CM/PT-CFAR achieves a higher detection probability than other CFAR algorithms when the SNR increases from 6 to 21 dB. In other words, the performance of CM/PT-CFAR is more robust than those of other CFAR algorithms.

For a more complex situation, two targets with different SNRs enter the clutter map successively and persist in different resolution cells. Figure 7 presents the performance of various CFAR algorithms to the weak target with

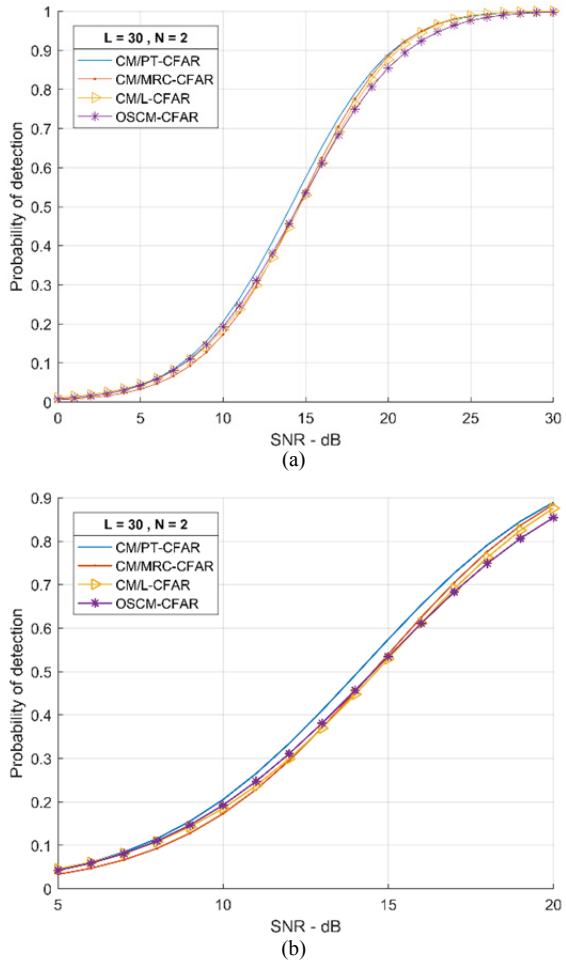

Fig. 6. Detection performance of various CFAR algorithms in the situation of two targets persisting for thirty scans: (a) global view; (b) partial curves for observation.

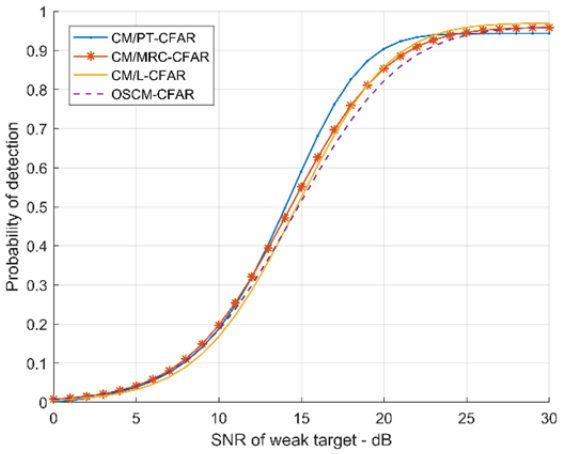

Fig. 7. Detection performance of various CFAR algorithms to weak persisting target.

a lower SNR. Assume that the weak target enters clutter map $\Delta L = 10$ scans later than the strong target, and the SNR of the weak target is half that of the strong target. CM/PT-CFAR shows obvious robustness for weak target detection when multiple targets enter the clutter map in sequence. The detection probability of CM/PT-CFAR to the weak target is higher than those of other CFAR algorithms in the SNR range from 12 to 23 dB.

4.2.3 Detection Performance versus Target Persisting Scans

The detection performance of various CFAR algorithms with respect to the number of persistence scans is presented in Fig. 8. On the curves of one persisting target with SNR = 20 dB, CM/MRC-CFAR achieves the highest detection probability, while CM/PT-CFAR performs better than CM/L-CFAR and OSCM-CFAR. In the case of a high SNR, CM/PT-CFAR obtains a relatively larger scale factor γ, which leads to fewer resolution cells used for updating the detection threshold than those of CM/MRC-CFAR. Thus, the detection probability of CM/PT-CFAR is lower than that of CM/MRC-CFAR. On the curves of two persisting targets with SNR = 15 dB, because the scale factor γ maintains slight fluctuation when SNR changes, CM/PT-CFAR utilizes more resolution cells to update the detection threshold than other CFAR algorithms. Therefore, the performance of CM/PT-CFAR shows more robust in this situation.

4.3 Synthetical Experiment

The previous sections mainly investigate the detection performance evaluation under the influence of various parameters (such as targets number, persisting scans) in different environments (homogeneous or nonhomogeneous). In this section, we focus on the detection performance for weak targets in complex situations, which is the original intention that CM/PT-CFAR algorithm was proposed. Four CM-CFAR detectors including CM/PT-CFAR, CM/MRC-CFAR, CM/L-CFAR, and OSCM-CFAR are tested under uniform conditions to sufficiently present their performance

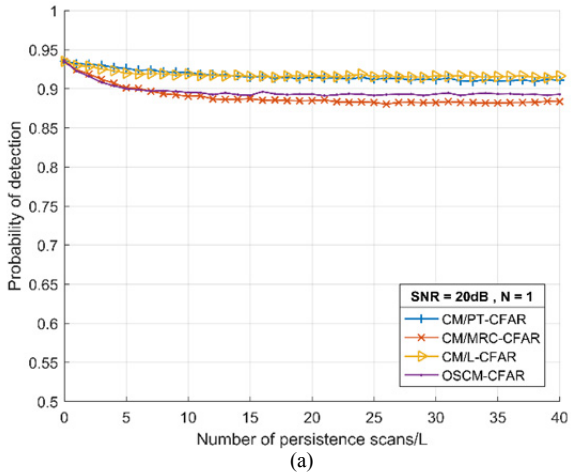

(a)

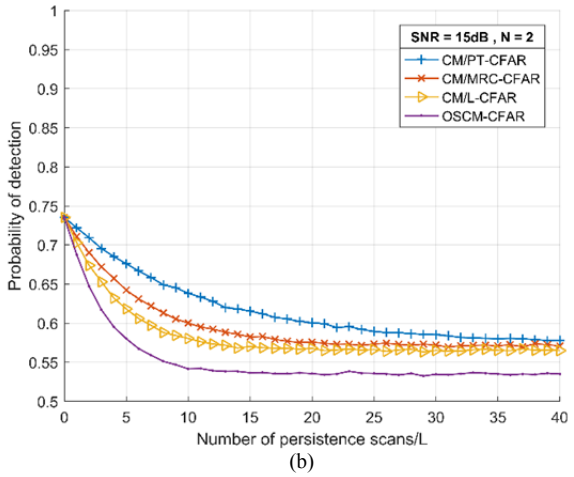

(b)

Fig. 8. Detection performance of various CFAR algorithms as number of targets persisting scans changes: (a) one target with SNR = 20 dB; (b) two targets with SNR = 15 dB.

Hardware configuration	CPU: Intel Xeon E5-2697 v4 @2.30GHz RAM: 192GB available
General parameters for four detectors	Clutter map size: $M = 16$ Desired $P_F = 1 \times 10^{-6}$ Fixed SNR: $\sigma = 20$dB
Parameter set of CM/PT-CFAR	Weight coefficient: $\alpha = 0.125$ Power exponent: $v = 0.2154$ Threshold factor: $T = 8.875$
Parameter set of CM/MRC-CFAR	Weight coefficient:$\alpha = 0.125$ Scaling factor: $\gamma = 0.33$ Threshold factor: $T = 17.503$ Target number tolerance: $M_T = 3$
Parameter set of CM/L-CFAR	Censoring depth: $r = 4$
Parameter set of OSCM-CFAR	Cell number for updating: 9th

Tab. 2. Parameter sets of four CFAR detectors and the hardware configuration.

comparison. Parameters of these detectors are redesigned and shown in Tab. 2. For CM/PT-CFAR, the design process is completely consistent with that in Sec. 4.1. As for another three detectors, the respective parameters are obtained according to [16], [17], and [19], which are not described in detail. In addition, the hardware configuration information is given in Tab. 2.

To compare the robustness of four detectors in complex environments, we simulate three different detection cases: (a) two targets with same signal-to-clutter ratio (SCR) of 10 dB enter the clutter map at the same time and persist for 20 scans, detect any one target; (b) a strong target (SCR = 10 dB) and a weak target (SCR = 0 dB) enter the clutter map at the same time and persist for 20 scans, detect the weak target; (c) a strong target (SCR = 10 dB) enters and persists in the clutter map, 20 scans later a weak target enters the clutter map, detect the weak target. In each of the three simulation cases, the receiver operating characteristic (ROC) curve is generated by Monte Carlo method to present the detection performance, as shown in Fig. 9. In addition, the time consumption is also recorded in Tab. 3.

	Case (a)	Case (b)	Case (c)
CM/PT-CFAR	238.266275s	241.568137s	240.157264s
CM/MRC-CFAR	187.651723s	237.264711s	262.556831s
CM/L-CFAR	241.368547s	253.573365s	247.338572s
OSCM-CFAR	302.685421s	331.258293s	327.772805s

Tab. 3. Time consumption of simulations.

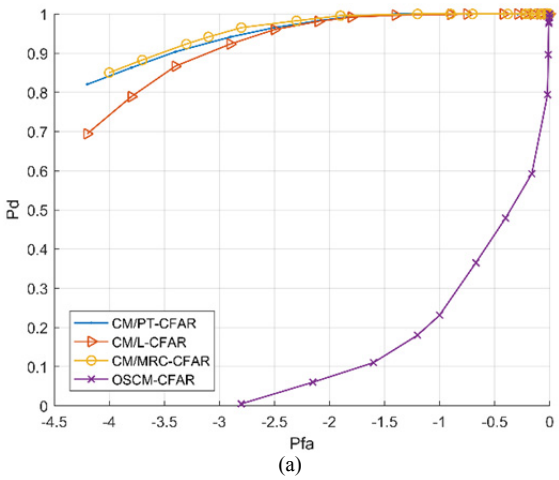

(a)

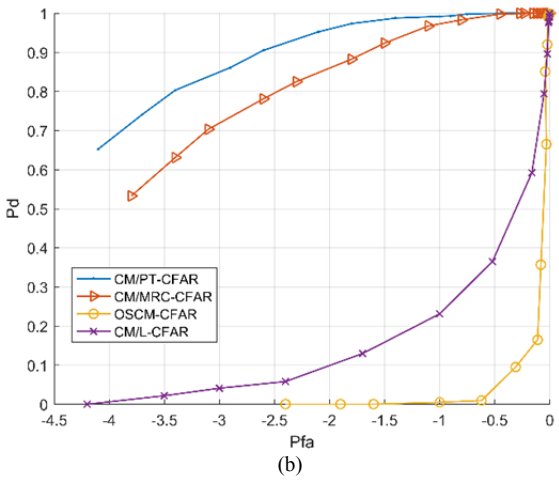

(b)

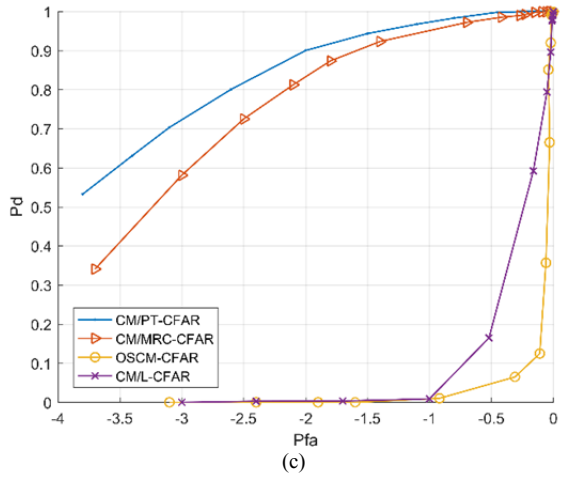

Fig. 9. The receiver operating characteristic (ROC) curves of different detectors in the three cases: (a) two identical targets enter the map concurrently; (b) a strong target with a weak target enter the map concurrently; (c) a strong target with a weak target enter the map successively.

For each detection case, the Monte Carlo experiment is implemented 100 000 times to calculate the false-alarm probability and detection probability, yielding the ROC curves. As shown in Fig. 9, CM/PT-CFAR achieves higher P_d than other CFAR detectors with the same P_F, whatever the case. Note that from cases (a) to (c), the corresponding detection situations get worse gradually, the ROC curve of CM/PT-CFAR shows more robustness than those of other detectors.

From Tab. 3 we can find that the time consumption of CM/PT-CFAR is relatively stable in three cases, while the time consumption of CM/MRC-CFAR has a significant fluctuation. This is because CM/PT-CFAR always takes partial elements of the radar dataset to update the detection threshold. In contrast, CM/MRC-CFAR's update strategy is affected by the intensity of target cells, and might use elements of the entire dataset in certain cases, leading to an increased computation. Ranking information is required for OSCM-CFAR algorithm, which results in an added computation load and more time consumptions.

4.4 Effect of Power Exponent *v* on CM/PT-CFAR Performance

For CM/PT-CFAR algorithm, the power exponent v is a key factor that adjusts the differences between echo intensity of the resolution cells. As the case shown in Sec. 4.1, it has a significant impact on the detection performance. In this section, the performance of CM/PT-CFAR conditioned on v is investigated, and the detection probability curves in two different situations are presented. The parameter set (M, P_F, α) is same as that in Sec. 4.1. To facilitate the calculation, v is chosen from set (1/2, 1/3, 1/4, 1/5, 1/6).

As shown in Fig. 10, in a homogeneous environment, when v increases from 1/6 to 1/2, the detection performance of CM/PT-CFAR improves significantly. Because the difference between the transformed target echo and clutter intensity increases with increasing power exponent v, it is more suitable to select a larger power exponent in the homogeneous environment.

When two targets with different SNRs enter the clutter map successively and persist in different resolution cells, the detection performance of CM/PT-CFAR is shown in Fig. 11. Assume that a weak target with half the SNR of the strong target enters the clutter map 10 scans later than the other one. On the curves of v = 1/2 to 1/4, the decrease of power exponent leads to the reduction of difference between the transformed targets echoes. Therefore, the masking effect of the strong target on the weak target is weakened, and the detection performance to the weak target is improved. Note that on the curve of v = 1/4, CM/PT-CFAR achieves a robust detection performance when the SNR is lower than 19 dB. For SNR at a higher level, because the target echo intensity greatly differs from the clutter intensity, CM/PT-CFAR will engender a negative effect on the resolution between the target and clutter. Therefore, the upper limit of detection probability is slightly reduced and maintains at approximately 94.9%. On the curves of v = 1/5 and v = 1/6, the detection performance is significantly

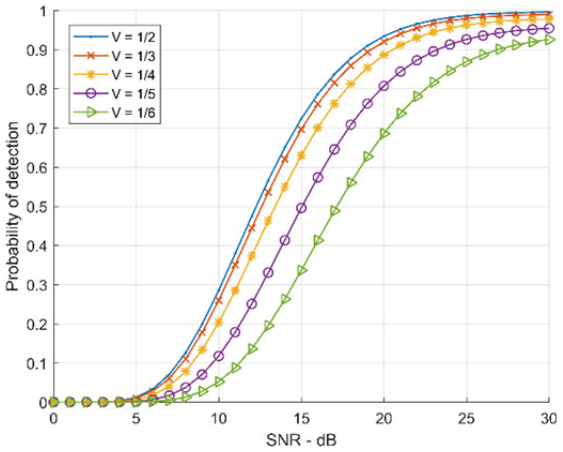

Fig. 10. Detection performance of CM/PT-CFAR with different values of v in a homogeneous environment.

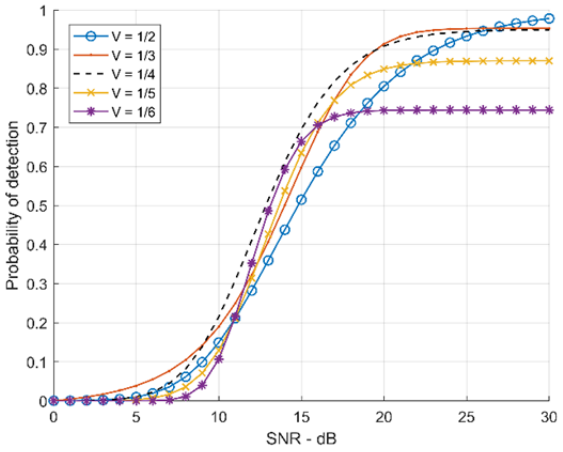

Fig. 11. Detection performance of CM/PT-CFAR with different values of v in two persisting targets situation.

deteriorated. This is because the power transform with a power exponent that is too small greatly reduces the difference between the target echo and clutter intensity.

5. Conclusions

CM/PT-CFAR utilizes a power transform operation to increase the separability between the target cells and the clutter cells, so as to reduce the masking effect caused by persisting targets and improve the detection performance for targets in the clutter map, especially for weak targets. For CM/PT-CFAR algorithm, a third-order Taylor expansion operation is used to approximate the closed-form of the detection probability. The detection performances of CM/PT-CFAR in different environments are investigated and compared with those of other CM-CFAR detectors. The results show that the proposed algorithm exhibits a low CFAR loss in a homogeneous clutter environment and achieves a robust detection performance for weak targets in the case of multiple persisting targets entering the radar scene. The power exponent has a significant impact on the detection performance of CM/PT-CFAR. A larger power exponent is more appropriate in the homogeneous environment, while the proper reduction of power exponent can increase the robustness of target detection in nonhomogeneous situations. It should be point out that the optimal power exponent is determined by enumeration method at present, which brings extra computation. Seeking for a better approach to the optimal parameter is authors' next work.

Acknowledgments

The authors thank the anonymous reviewers for their constructive suggestions to improve this paper. This work was supported by the National Natural Science Foundation of China (61801221, 62001229).

References

[1] SKOLNIK, M. I. *Introduction to Radar Systems*. New York (US): McGraw-Hill, 1990. ISBN: 0-07-057909-1

[2] SHNIDMAN, D. A. Radar detection in clutter. *IEEE Transactions on Aerospace and Electronic Systems*, 2005, vol. 41, no. 3, p. 1056–1067. DOI: 10.1109/TAES.2005.1541450

[3] FINN, H. M., JOHNSON, R. S. Adaptive detection mode with threshold control as a function of spatially sampled clutter level estimates. *RCA Review*, 1968, p. 414–464.

[4] FINN, H. M. A CFAR design for a window spanning two clutter fields. *IEEE Transactions on Aerospace and Electronic Systems*, 1986, vol. AES-22, no. 2, p. 155–169. DOI: 10.1109/TAES.1986.310750

[5] WEISS, M. Analysis of some modified cell-averaging CFAR processors in multiple-target situations. *IEEE Transactions on Aerospace and Electronic Systems*, 1982, vol. AES-18, no. 1, p. 102–114. DOI: 10.1109/TAES.1982.309210

[6] HAMMOUDI, Z., SOLTANI, F. Distributed CA-CFAR and OS-CFAR detection using fuzzy spaces and fuzzy fusion rules. *IEE Proceedings - Radar Sonar and Navigation,* 2004, vol. 151, no. 3, p. 135–142. DOI: 10.1049/ip-rsn:20040560

[7] BARKAT, M., FARROUKI, A. Automatic censoring CFAR detector based on ordered data variability for nonhomogeneous environments. *IEE Proceedings - Radar, Sonar and Navigation*, 2005, vol. 152, no. 1, p. 43–51. DOI: 10.1049/ip-rsn:20045006

[8] CAO, T. V. Constant false-alarm rate algorithm based on test cell information. *IET - Radar Sonar and Navigation,* 2008, vol. 2, no. 3, p. 200–213. DOI: 10.1049/iet-rsn:20070133

[9] MENG, X. W. Performance analysis of ordered-statistic greatest of-constant false alarm rate with binary integration for M-sweeps. *IET - Radar Sonar and Navigation*, 2010, vol. 4, no, 1, p. 37–48. DOI: 10.1049/iet-rsn.2008.0119

[10] SHAN, T., TAO, R., WANG, Y., et al. Novel clutter map CFAR algorithm with amplitude limiter. *Journal of Systems Engineering and Electronics*, 2004, vol. 15, no. 3, p. 262–265.

[11] LOPS, M., ORSINI, M. Scan-by-scan averaging CFAR. *IEE Proceedings F - Radar and Signal Processing*, 1989, vol. 136, no. 6, p. 249–254. DOI: 10.1049/ip-f-2.1989.0038

[12] CONTE, E., LOPS, M. Clutter-map CFAR detection for range-spread targets in non-Gaussian clutter. I. System design. *IEEE Transactions on Aerospace and Electronic Systems*, 1997, vol. 33, no. 2, p. 432–443. DOI: 10.1109/7.575877

[13] CONTE, E., DI BISCEGLIE, M., LOPS, M. Clutter-map CFAR detection for range-spread targets in non-Gaussian clutter. II. Performance assessment. *IEEE Transactions on Aerospace and Electronic Systems*, 1997, vol. 33, no. 2, p. 444–455. DOI: 10.1109/7.575879

[14] NITZBERG, R. Clutter Map CFAR Analysis. *IEEE Transactions on Aerospace and Electronic Systems*, 1986, vol. AES-22, no. 4, p. 419–421. DOI: 10.1109/TAES.1986.310777

[15] MA, J., WU, L., XU, S. T., et al. A new type CFAR detector based on censored mean and cell average. In *Sino-foreign-interchange Conference on Intelligent Science & Intelligent Data Engineering*. Xi'an (China), 2011, p. 706–712. DOI: 10.1007/978-3-642-31919-8_90

[16] SHAN, T., TAO, R., WANG, Y., et al. Performance of order statistic clutter map CFAR. In *6th International Conference on Signal Processing*. Beijing (China), 2002, p. 1572–1575. DOI: 10.1109/ICOSP.2002.1180097

[17] LOPS, M. Hybrid clutter-map/L-CFAR procedure for clutter rejection in nonhomogeneous environment. *IEE Proceedings - Radar Sonar and Navigation*, 1996, vol. 143, no. 4, p. 239–245. DOI: 10.1049/ip-rsn:19960212

[18] GURAKAN, B., CANDAN, Ç., ÇILOĞLU, T. CFAR processing with switching exponential smoothers for nonhomogeneous environments. *Digital Signal Processing*, 2012, vol. 22, no. 3, p. 407–416. DOI: 10.1016/j.dsp.2012.01.007

[19] ZHANG, R. L., SHENG, W. X., MA, X. F., et al. Clutter map CFAR detector based on maximal resolution cell. *Signal Image and Video Processing*, 2013, vol. 9, no. 5, p. 1151–1162. DOI: 10.1007/s11760-013-0544-0

[20] MENG, X. W. Performance analysis of Nitzberg's clutter map for Weibull distribution. *Digital Signal Processing*, 2010, vol. 20, no. 3, p. 916–922. DOI: 10.1016/j.dsp.2009.10.001

[21] HAMADOUCHE, M., BARAKAT, M., KHODJA, M. Analysis of the clutter map CFAR in Weibull clutter. *Signal Processing*, 2000, vol. 80, no. 1, p. 117–123. DOI: 10.1016/S0165-1684(99)00115-2

[22] ANASTASSOPOULOS, V., LAMPROPOULOS, G. A. Optimal CFAR detection in Weibull clutter. *IEEE Transactions on Aerospace and Electronic Systems*, 1995, vol. 31, no. 1, p. 52–64, DOI: 10.1109/7.366292

[23] ALMEIDA GARCÍA, F. D., FLORES RODRIGUEZ, A. C., FRAIDENRAICH, G., et al. CA-CFAR detection performance in homogeneous Weibull clutter. *IEEE Geoscience and Remote Sensing Letters*, 2018, vol. 16, no. 6, p. 887–891. DOI: 10.1109/LGRS.2018.2885451

[24] MENG, X. W. Performance of clutter map with binary integration against Weibull background. *AEUE - International Journal of Electronics and Communications*, 2013, vol. 67, no. 7, p. 611–615. DOI: 10.1016/j.aeue.2013.01.001

[25] RAGHAVAN, R. S. A CFAR detector for mismatched eigenvalues of training sample covariance matrix. *IEEE Transactions on Signal Processing*, 2019, vol. 67, no. 17, p. 4624–4635. DOI: 10.1109/TSP.2019.2929942

[26] AKÇAPINAR, K., BAYKUT, S. CM-CFAR parameter learning based square-law detector for foreign object debris radar. In *15th European Radar Conference (EuRAD)*. Madrid (Spain), 2018, p. 421–424. DOI: 10.23919/EuRAD.2018.8546514

[27] LIU, Y., ZHANG, S. F., SUO, J. D., et al. Research on a new comprehensive CFAR (Comp-CFAR) processing method. *IEEE Access*, 2019, vol. 7, p. 19401–19413. DOI: 10.1109/ACCESS.2019.2897358

[28] TAO, D., ANFINSEN, S. N., BREKKE, C. Robust CFAR detector based on truncated statistics in multiple-target situations. *IEEE Transactions on Geoscience and Remote Sensing*, 2016, vol. 54, no. 1, p. 117–134. DOI: 10.1109/TGRS.2015.2451311

[29] KRONAUGE, M., ROHLING, H. Fast two-dimensional CFAR procedure. *IEEE Transactions on Aerospace and Electronic Systems*, 2013, vol. 49, no. 3, p. 1817–1823. DOI: 10.1109/TAES.2013.6558022

[30] WEI, S. H., WANG, X. J. Research of CMLD-CFAR detecting algorithm in radar reconnaissance receiver. In *International Conference on Measuring Technology and Mechatronics Automation*. Zhangjiajie (China), 2009, p. 105–108. DOI: 10.1109/ICMTMA.2009.115

About the Authors

Bangzhen XU was born in HuBei, China. He received his B.E. degree from the School of Electronic and Optical Engineering, Nanjing University of Science and Technology in 2014. He is currently working towards the Ph.D. degree in Information and Communication Engineering at Nanjing University of Science and Technology. His main research interests include low altitude target detection and clutter suppression.

Yiqin CHEN received the Ph.D. degree from the School of Optical and Electronic Information, Huazhong University of Science and Technology in 2015. He is currently a postdoctor in the School of Electronic and Optical Engineering, Nanjing University of Science and Technology. His current research interests include algorithm development for target detection and tracking in mmwave radar and system integration.

Hong GU (corresponding author) received the M.S. degree from the Nanjing University of Science and Technology, Jiangsu, China, in 1991, and the Ph.D. degree from XIDIAN University, Shanxi, China, in 1995, both in Information and Communication Engineering. He is currently a Professor with the Nanjing University of Science and Technology, a Chinese Institute of Electronics Senior Member, and a member of radar branch of the Jiang Electronic Society. His research interests include noise SAR, radar signal processing, and information systems.

Weimin SU received the Ph.D. degree in Information and Communication Engineering from the Nanjing University of Science and Technology, Nanjing, China, in 1998. He is currently a Professor with the Nanjing University of Science and Technology, a Senior Member of the Chinese Institute of Electronics, and a Member of the Signal Processing Society of China. His research interests include signal processing technology and advanced SAR systems.

Appendix A:

The derivation of the pdf of random variable Z is essentially to solve the distribution of a random variable function. Variable X in the original radar data vector $\boldsymbol{x}$ has the pdf as follows:

$$f_X(x) = \frac{1}{\lambda(1+\sigma)} \mathrm{e}^{-x/\lambda(1+\sigma)}, x \geq 0. \tag{A1}$$

The scale transformation operation is realized by mapping elements of vector $\boldsymbol{x}$ into vector $\boldsymbol{y}$ through a linear function $Y = \alpha X$, where α is a positive constant. Obviously, variable Y has the same form of pdf as variable X:

$$f_Y(y) = \frac{1}{\lambda(1+\sigma)} \mathrm{e}^{-y/\lambda(1+\sigma)}, y \geq 0. \tag{A2}$$

Variable Z is the random variable function of variable Y, and it has $Z = Y^v$, $0 < v \leq 1$. The distribution function $F_Z(z)$ of Z is obtained as follows:

$$\begin{aligned} F_Z(z) &= P\{Z \leq z\} \\ &= P\{Y^v \leq z\} \\ &= P\{0 < Y \leq z^{1/v}\} \\ &= F_Y(z^{1/v}) - F_Y(0), \end{aligned}$$

and the pdf of Z is the derivative of $F_Z(z)$:

$$\begin{aligned} f_Z(z) &= F_Z'(z) \\ &= \mathrm{d}\left(F_Y(z^{1/v}) - F_Y(0)\right)/\mathrm{d}z \\ &= \frac{z^{(1-v)/v}}{\lambda v(1+\sigma)} \mathrm{e}^{-z^{(1/v)}/\lambda(1+\sigma)}. \end{aligned} \tag{A3}$$

Appendix B:

According to (14), the expression of $\Phi_I(t \mid m_0, l, zt_N \geq zc_{M-N})$ can be derived as follows:

$\Phi_I(t \mid m_0, l, zt_N \geq zc_{M-N}) =$

$$
\begin{aligned}
&= \int_0^{+\infty}\int_1^{zt_N}\int_1^{zt_{N-1}}\cdots\int_1^{zt_{l+2}}\int_0^{1}\int_0^{zt_l}\cdots\int_0^{zt_3}\int_0^{zt_2}\int_1^{zt_N}\int_1^{zc_{M-N}}\cdots\int_1^{zc_{m_0-l+2}}\int_0^{1}\int_0^{zc_{m_0-l}}\cdots\int_0^{zc_3}\int_0^{zc_2} N!(M-N)! \\
&\times\prod_{i=1}^{N} f_T(zt_i)\cdot\prod_{j=1}^{M-N} f_C(zc_j)\cdot \mathrm{e}^{-(zt_1+zt_2+\cdots+zt_N+zc_1+zc_2+\cdots+zc_{M-N})t} \\
&\quad\times \mathrm{d}_{zt_1}\mathrm{d}_{zt_2}\cdots\mathrm{d}_{zt_N}\mathrm{d}_{zc_1}\mathrm{d}_{zc_2}\cdots\mathrm{d}_{zc_{M-N}} \\
&= \int_0^{+\infty}\int_1^{zt_N}\int_1^{zt_{N-1}}\cdots\int_1^{zt_{l+2}}\int_0^{1}\int_0^{zt_l}\cdots\int_0^{zt_3}\int_0^{zt_2}\int_1^{zt_N}\int_1^{zc_{M-N}}\cdots\int_1^{zc_{m_0-l+2}}\int_0^{1}\int_0^{zc_{m_0-l}}\cdots\int_0^{zc_3}\int_0^{zc_2} N!(M-N)! \\
&\times\prod_{i=1}^{N}\left\{\frac{(zt_i)^{\frac{1-v}{v}}}{\lambda v(1+\sigma)}\cdot\exp\left[\frac{-(zt_i)^{\frac{1}{v}}}{\lambda v(1+\sigma)}-zt_i\cdot t\right]\right\} \\
&\times\prod_{j=1}^{M-N}\left\{\frac{(zc_j)^{\frac{1-v}{v}}}{\lambda v}\cdot\exp\left[\frac{-(zc_j)^{\frac{1}{v}}}{\lambda v}-zc_j\cdot t\right]\right\} \\
&\times \mathrm{d}_{zt_1}\mathrm{d}_{zt_2}\cdots\mathrm{d}_{zt_N}\mathrm{d}_{zc_1}\mathrm{d}_{zc_2}\cdots\mathrm{d}_{zc_{M-N}}\ .
\end{aligned}
\tag{B1}
$$

Note that (B1) is a transcendental integral whose analytic expression cannot be accurately obtained. This is because the pdf as an integrand is turned into a non-elementary function by the power transform. Here, a third-order Taylor expansion operation is applied to (15) and (16), leading to the following expression:

$$
\begin{aligned}
&f_T(z) = \\
&\frac{(z)^{\frac{1-v}{v}}}{\lambda v(1+\sigma)}-\frac{(z)^{\frac{2-v}{v}}}{\lambda^2 v(1+\sigma)^2}+\frac{(z)^{\frac{3-v}{v}}}{2\lambda^3 v(1+\sigma)^3}-\frac{(z)^{\frac{4-v}{v}}}{6\lambda^4 v(1+\sigma)^4} \\
&+o\left((z)^{\frac{4-v}{v}}\right),
\end{aligned}
\tag{B2}
$$

$$
f_C(z)=\frac{(z)^{\frac{1-v}{v}}}{\lambda v}-\frac{(z)^{\frac{2-v}{v}}}{\lambda^2 v}+\frac{(z)^{\frac{3-v}{v}}}{2\lambda^3 v}-\frac{(z)^{\frac{4-v}{v}}}{6\lambda^4 v}+o\left((z)^{\frac{4-v}{v}}\right)\cdot \tag{B3}
$$

Combined with (B2) and (B3), Equation (B1) can be rewritten in the following approximate form:

$$
\begin{aligned}
&\Phi_I(t\,|\,m_0,l,zt_N\ge zc_{M-N}) \\
&\approx\frac{N!(M-N)!}{(m_0-l)!(M-N-m_0+l)!l!(N-l-1)!}\cdot\left(1+\frac{t}{\lambda v}\right)^{-(M-N)} \\
&\times\left(1+\frac{t}{\lambda v(1+\sigma)}\right)^{-(N-1)}\cdot\sum_{i}^{m_0-l}\sum_{j}^{M-N-m_0+l}\sum_{u}^{l}\sum_{w}^{N-l-1}\binom{m_0-l}{i} \\
&\times\binom{M-N-m_0+l}{j}\cdot\binom{l}{u}\cdot\binom{N-l-1}{w}\cdot\left(1+\frac{\lambda(1+\sigma)}{t}\right)^{\frac{1}{v}}\cdot\left(1+\frac{\lambda}{t}\right)^{\frac{1}{v}} \\
&\times\Gamma\left(\frac{t}{\lambda v(1+\sigma)},\frac{1}{v}\right)\cdot\Gamma\left(\frac{t}{\lambda v},\frac{1}{v}\right) \\
&\times\exp\left\{\frac{t}{\left[\lambda v(1+\sigma)+1\right]\lambda v r_1+(\lambda v+1)\lambda v(1+\sigma)r_2}\right\}
\end{aligned}
\tag{B4}
$$

where

$$
\begin{aligned}
r_1 &= v(i+M-N-m_0+l)+(1-v)j\ , \\
r_2 &= v(u+N-l-1)+(1-v)w+1\cdot
\end{aligned}
$$

In addition, $\Gamma(a,b)$ denotes the incomplete gamma function of variables a and b.

Using a similar approach, we can derive the approximate expression of $\Phi_I(t\,|\,m_0,l,zt_N<zc_{M-N})$ as follows:

$$
\begin{aligned}
&\Phi_I(t\,|\,m_0,l,zt_N<zc_{M-N}) \\
&\approx\frac{N!(M-N)!}{l!(N-l)!(m_0-l)!(M-N-m_0+l-1)!}\cdot\left(1+\frac{t}{\lambda v(1+\sigma)}\right)^{-N} \\
&\times\left(1+\frac{t}{\lambda v}\right)^{-(M-N-1)}\cdot\sum_{i}^{l}\sum_{j}^{N-l}\sum_{u}^{m_0-l}\sum_{w}^{M-N-m_0+l-1}\binom{l}{i}\cdot\binom{N-l}{j} \\
&\times\binom{m_0-l}{u}\cdot\binom{M-N-m_0+l-1}{w}\cdot\left(1+\sigma+\frac{\lambda}{t}\right)^{\frac{1}{v}}\cdot\left(1+\frac{\lambda}{t}\right)^{\frac{1}{v}} \\
&\times\Gamma\left(\frac{(1+\sigma)t}{\lambda v+1+\sigma},\frac{1}{v}\right)\cdot\Gamma\left(\frac{t}{\lambda v+1},\frac{1}{v}\right) \\
&\times\exp\left\{\frac{t}{\left[\lambda v+1+\sigma\right]\lambda v r_3+(\lambda v+1)\lambda v(1+\sigma)^{-1}r_4}\right\}
\end{aligned}
\tag{B5}
$$

where

$$
\begin{aligned}
r_3 &= v(i+N-l)+(1-v)j\ , \\
r_4 &= v(u+M-N-m_0+l-1)+(1-v)w+1\ .
\end{aligned}
$$

Substituting (B4) and (B5) into (17), the expression of $\Phi_{qI}(t)$ is obtained as follows:

$$
\begin{aligned}
&\Phi_{qI}(t)=\sum_{m_0=0}^{M-1}\sum_{l=N_0}^{N_1}\frac{N!(M-N)!}{(m_0-l)!(M-N-m_0+l)!l!(N-l-1)!} \\
&\times\left(1+\frac{t}{\lambda v}\right)^{-(M-N)}\cdot\left(1+\frac{t}{\lambda v(1+\sigma)}\right)^{-(N-1)} \\
&\times\sum_{i}^{m_0-l}\sum_{j}^{M-N-m_0+l}\sum_{u}^{l}\sum_{w}^{N-l-1}\binom{m_0-l}{i}\cdot\binom{M-N-m_0+l}{j} \\
&\times\binom{l}{u}\cdot\binom{N-l-1}{w}\cdot\left(1+\frac{\lambda(1+\sigma)}{t}\right)^{\frac{1}{v}}\cdot\left(1+\frac{\lambda}{t}\right)^{\frac{1}{v}} \\
&\times\Gamma\left(\frac{t}{\lambda v(1+\sigma)},\frac{1}{v}\right)\cdot\Gamma\left(\frac{t}{\lambda v},\frac{1}{v}\right) \\
&\times\exp\left\{\frac{t}{\left[\lambda v(1+\sigma)+1\right]\lambda v r_1+(\lambda v+1)\lambda v(1+\sigma)r_2}\right\} \\
&+\sum_{m_0=0}^{M-1}\sum_{l=N_2}^{N_3}\frac{N!(M-N)!}{l!(N-l)!(m_0-l)!(M-N-m_0+l-1)!} \\
&\times\left(1+\frac{t}{\lambda v(1+\sigma)}\right)^{-N}\cdot\left(1+\frac{t}{\lambda v}\right)^{-(M-N-1)} \\
&\times\sum_{i}^{l}\sum_{j}^{N-l}\sum_{u}^{m_0-l}\sum_{w}^{M-N-m_0+l-1}\binom{l}{i}\cdot\binom{N-l}{j} \\
&\times\binom{m_0-l}{u}\cdot\binom{M-N-m_0+l-1}{w}\cdot\left(1+\sigma+\frac{\lambda}{t}\right)^{\frac{1}{v}}\cdot\left(1+\frac{\lambda}{t}\right)^{\frac{1}{v}}
\end{aligned}
$$

$$\times\Gamma\left(\frac{(1+\sigma)t}{\lambda v+1+\sigma},\frac{1}{v}\right)\cdot\Gamma\left(\frac{t}{\lambda v+1},\frac{1}{v}\right)$$

$$\times\exp\left\{\frac{t}{\left[\lambda v+1+\sigma\right]\lambda v r_3+(\lambda v+1)\lambda v(1+\sigma)^{-1}r_4}\right\}. \quad \text{(B6)}$$

The derivation of $\Phi_{qH}(t)$ is similar to that of $\Phi_{qI}(t)$. Note that since the clutter map is in a homogeneous environment, we set $N = 0$ and $\sigma = 0$, thus obtaining the following expression:

$$\Phi_{qH}(t)=\sum_{m_0=0}^{M-1}\frac{M!}{m_0!(M-m_0-1)!}\cdot\left(1+\frac{t}{\lambda v}\right)^{(1-M)}$$

$$\times\sum_{i=0}^{m_0}\sum_{j=0}^{M-m_0-1}\binom{m_0}{i}\cdot\binom{M-m_0-1}{j}$$

$$\times\left(1+\frac{\lambda}{t}\right)^{\frac{2}{v}}\cdot\left[\Gamma\left(\frac{t}{\lambda v+1},\frac{1}{v}\right)\right]^2\cdot\exp\left\{\frac{-t}{(\lambda v+1)\lambda v\left(r_1^{'}+r_2^{'}\right)}\right\}$$

$$+\sum_{m_0=0}^{M-1}\frac{M!}{m_0!(M-m_0-1)!}\cdot\left(1+\frac{t}{\lambda v}\right)^{(1-M)}$$

$$\times\sum_{i=0}^{m_0}\sum_{j=0}^{M-m_0-1}\binom{m_0}{i}\cdot\binom{M-m_0-1}{j}$$

$$\times\left(1+\frac{\lambda}{t}\right)^{\frac{2}{v}}\cdot\left[\Gamma\left(\frac{t}{\lambda v+1},\frac{1}{v}\right)\right]^2\cdot\exp\left\{\frac{-t}{(\lambda v+1)\lambda v\left(r_3^{'}+r_4^{'}\right)}\right\} \quad \text{(B7)}$$

where

$$r_1^{'}=(1-v)w+v(N-m-1),$$

$$r_2^{'}=(1-v)j+v(M-N-m_0+m-1)+1,$$

$$r_3^{'}=(1-v)w+v(M-N-m_0+m-1)+1,$$

$$r_4^{'}=(1-v)j+v(N-m).$$

Substituting (B6), (B7), and (13) into (11), the expression of P_{d} is obtained as follows:

$$P_{\mathrm{d}}=\Phi_{\hat{p}(n+L)}(t)\big|_{t=\frac{T}{\lambda(1+\sigma)}}$$

$$=\prod_{k=0}^{L-1}\left\{\sum_{m_0}^{M-1}\sum_{l=N_0}^{N_1}\frac{N!(M-N)!}{(m_0-l)!(M-N-m_0+l)!l!(N-l-1)!}\cdot\left[1+\frac{\alpha(1-\alpha)^k T}{v(1+\sigma)}\right]^{(N-M)}\cdot\left[1+\frac{\alpha(1-\alpha)^k T}{v(1+\sigma)^2}\right]^{(1-N)}\right.$$

$$\times\sum_{i}^{m_0-l}\sum_{j}^{M-N-m_0+l}\sum_{u}^{l}\sum_{w}^{N-l-1}\binom{m_0-l}{i}\cdot\binom{M-N-m_0+l}{j}\cdot\binom{l}{u}\cdot\binom{N-l-1}{w}\cdot\left[1+\frac{(1+\sigma)^2}{\alpha(1-\alpha)^k T}\right]^{\frac{1}{v}}\cdot\left[1+\frac{(1+\sigma)}{\alpha(1-\alpha)^k T}\right]^{\frac{1}{v}}$$

$$\times\Gamma\left[\frac{\alpha(1-\alpha)^k T}{(1+\sigma)\left[1+v(1+\sigma)\right]},\frac{1}{v}\right]\cdot\Gamma\left[\frac{\alpha(1-\alpha)^k T}{(1+\sigma)(1+v)},\frac{1}{v}\right]\cdot\exp\left[\frac{-\alpha(1-\alpha)^k T}{\left[1+v(1+\sigma)\right]v(1+\sigma)r_1+(1+v)v(1+\sigma)^2 r_2}\right]$$

$$+\sum_{m_0}^{M-1}\sum_{l=N_2}^{N_3}\frac{N!(M-N)!}{l!(N-l)!(m_0-l)!(M-N-m_0+l-1)!}\cdot\left[1+\frac{\alpha(1-\alpha)^k T}{v(1+\sigma)^2}\right]^{-N}\cdot\left[1+\frac{\alpha(1-\alpha)^k T}{v(1+\sigma)}\right]^{(1+N-M)}$$

$$\times\sum_{i}^{l}\sum_{j}^{N-l}\sum_{u}^{m_0-l}\sum_{w}^{M-N-m_0+l-1}\binom{l}{i}\cdot\binom{N-l}{j}\cdot\binom{m_0-l}{u}\cdot\binom{M-N-m_0+l-1}{w}\cdot\left[1+\sigma+\frac{1+\sigma}{\alpha(1-\alpha)^k T}\right]^{\frac{1}{v}}\cdot\left[1+\frac{1+\sigma}{\alpha(1-\alpha)^k T}\right]^{\frac{1}{v}}$$

$$\left.\times\Gamma\left[\frac{\alpha(1-\alpha)^k T}{(1+v+\sigma)},\frac{1}{v}\right]\cdot\Gamma\left[\frac{\alpha(1-\alpha)^k T}{(1+\sigma)(1+v)},\frac{1}{v}\right]\cdot\exp\left[\frac{-\alpha(1-\alpha)^k T}{(1+v+\sigma)v(1+\sigma)r_3+(1+v)v\sigma r_4}\right]\right\}$$

$$\times\prod_{k=L}^{+\infty}\left\{\sum_{m_0=0}^{M-1}\frac{M!}{m_0!(M-m_0-1)!}\cdot\left[1+\frac{\alpha(1-\alpha)^k T}{v(1+\sigma)}\right]^{(1-M)}\cdot\sum_{i=0}^{m_0}\sum_{j=0}^{M-m_0-1}\binom{m_0}{i}\cdot\binom{M-m_0-1}{j}\right.$$

$$\times\left[1+\frac{(1+\sigma)}{\alpha(1-\alpha)^k T}\right]^{\frac{2}{v}}\cdot\left[\Gamma\left(\frac{\alpha(1-\alpha)^k T}{(1+\sigma)(1+v)},\frac{1}{v}\right)\right]^2\cdot\exp\left[\frac{-\alpha(1-\alpha)^k T}{v(1+v)(1+\sigma)\left(r_1^{'}+r_2^{'}\right)}\right]$$

$$+\sum_{m_0=0}^{M-1}\frac{M!}{m_0!(M-m_0-1)!}\cdot\left[1+\frac{\alpha(1-\alpha)^k T}{v(1+\sigma)}\right]^{(1-M)}\cdot\sum_{i=0}^{m_0}\sum_{j=0}^{M-m_0-1}\binom{m_0}{i}\cdot\binom{M-m_0-1}{j}$$

$$\left.\times\left[1+\frac{(1+\sigma)}{\alpha(1-\alpha)^k T}\right]^{\frac{2}{v}}\cdot\left[\Gamma\left(\frac{\alpha(1-\alpha)^k T}{(1+\sigma)(1+v)},\frac{1}{v}\right)\right]^2\cdot\exp\left[\frac{-\alpha(1-\alpha)^k T}{v(1+v)(1+\sigma)\left(r_3^{'}+r_4^{'}\right)}\right]\right\}. \quad \text{(B8)}$$